

FORCE SENSORS FOR
HUMAN/ROBOT INTERACTION

by

William Andrew Lorenz

A thesis submitted to the faculty of
Northwestern University
in partial fulfillment of the requirements for the degree of

Master of Science
in
Mechanical Engineering

Department of Mechanical Engineering

Northwestern University

July 1999

Table of Contents

ABSTRACT	III
ACKNOWLEDGMENTS	IV
1. INTRODUCTION	1
2. BENEFITS OF RELAXED DESIGN REQUIREMENTS	2
2.1 LARGER DEFLECTIONS	2
2.2 FEWER DEGREES OF FREEDOM	3
3. DESIGN	4
3.1 PHYSICAL OVERVIEW	4
3.1.1 <i>Optoelectronic sensor</i>	5
3.1.2 <i>Electromagnetic sensor</i>	8
3.2 COMPLIANCE MATRIX	9
3.3 DECOUPLING OF AXES	12
3.3.1 <i>Flexure properties</i>	13
3.3.2 <i>Displacement sensor properties</i>	14
3.3.3 <i>Human interface design</i>	14
3.4 PARAMETER SELECTION/MATERIAL SELECTION	14
3.4.1 <i>In-plane force analysis</i>	15
3.4.2 <i>More complete force analysis</i>	18
3.4.3 <i>Bending due to out of plane forces</i>	18
3.4.4 <i>Stresses due to all applied forces</i>	19
3.4.5 <i>Results, how to determine size parameters based on design constraints</i>	20
3.4.6 <i>Material considerations</i>	23
4. ALTERNATIVE FLEXURE DESIGNS	27
5. EXPERIMENTAL RESULTS	30
5.1 DEFLECTION	32
5.2 NOISE AND DRIFT	32
5.3 LINEARITY	32
5.4 RESPONSE TO OUT OF PLANE FORCES	34
5.5 EXPERIMENTAL SUMMARY	35
6. SUMMARY	35
APPENDIX	38

Abstract

Conventional force sensors are overdesigned for use in measuring human force inputs, such as is needed in research and application of human/robot interaction. A new class of force sensors is introduced that is suited to human-robot interaction. The sensor allows larger displacements in response to forces than present commercial sensors, and orthogonalizes the axes to be measured by a combination of the properties of the flexure and the displacement sensing mechanism. Two methods of measuring the displacement, optoelectronic and electromagnetic, are discussed. Criteria for material selection and dimensioning are given, and experimental results are reported.

Acknowledgments

I would like to thank Professor Michael Peshkin for his help in developing many of the ideas of this thesis, for his guidance and counsel, and for the opportunity to apply for my first patent. I would like to thank Professor Ed Colgate for his help and guidance. Also thanks to Mike Brown, Bernie Reger, Carl Moore and Julio Santos-Munné, for their patience to my initial flood of questions upon arriving at Northwestern. Thanks to all the members of LIMS for their support and friendship. I would like to thank Rich Dojutrek and Jesse Havens for teaching me a small part of what they know about machining. I would like to thank my parents and family, without which I wouldn't be here. I would like to thank God for the opportunity to do this work.

1. Introduction

The purpose of this thesis is to present a force sensor design that is less expensive and easier to construct than existing force sensors, but still has enough resolution, linearity and robustness to be used in a wide variety of applications. It is specifically designed with the requirements of human-robot interaction in mind. It can be utilized in such areas as human-robot coordination, ([3],[4]) teleoperation ([5]), and collaborative robots ([1],[2]).

In most situations where humans are applying forces, they are not sensitive to deflections on the order of a millimeter, and yet commercial force sensors deflect much less than this. In addition, there are many situations where only a few axes of human input are required. Yet most multi-axis force sensors are designed to measure all six axes.

Many force sensors must use many individual sensors to find one component of the applied force. To find how these sensors combine to give force components, each new force sensor must be calibrated, and a calibration matrix determined. The force sensor presented here is designed such that measurements of different force components are independent. Thus only one individual sensor is needed to measure one component of force.

Presently, commercial force sensors cost thousands of dollars. By allowing larger deflections and measuring fewer degrees of freedom, it becomes possible to design a much less expensive force sensor. It is hard at this point to estimate the cost to produce the force sensors presented here, but it is believed that the Lexan force sensor, which could be injection-molded, could be made for well under \$100. All electronic components for the sensing mechanisms are very cheap. The tolerances of construction are large. Calibration is trivial and takes under a minute.

2. Benefits of relaxed design requirements

Human-robot interaction requires different properties of a force sensor than typical robot applications such as machining and assembly. These differences have substantial impact on how a force sensor can be designed.

2.1 Larger deflections

Humans are relatively insensitive to small displacements on the order of a millimeter. These same displacements would cause trouble if they occurred at the end effector of a robot, which can be thought of as needing (or benefiting from) the accuracy of a machine tool such as a mill. So what advantages are obtained by loosening the restrictions on how much displacement is allowed?

Presently, strain gauges are used in most commercially available force sensors. Strain gauges measure the very slight bend of a flexure element caused by applied forces. However, they are difficult to install and calibrate and are easy to break. While the strain gauge elements themselves are inexpensive, in practice their difficulty of application results in sensors costing thousands of dollars.

The allowance of larger deflections allows the use of new kinds of sensors which have advantages. In the design presented here, two such sensors have been implemented. The first is optoelectronic in nature. Infrared LED/photodiode pairs are used as the sensor element in place of strain gauges. Strain gauges can measure deflections on the order of microns, and so are applied to very stiff flexure elements. Photosensors can be used to measure deflections on the order of millimeters, and thus are applied to much more compliant flexures. Photosensors suffer from some of the same problems as strain gauges, including nonlinearity and temperature

sensitivity. However, these have distinct advantages. Photosensors are cheap, easy to mount, are a non-contact sensor element, and are relatively hard to break. It should be noted here that other force sensor designs using optoelectronic devices exist. ([8])

The second displacement sensing device is electromagnetic in nature. Two zigzags of conducting material slide past each other. An AC current is applied to one zigzag, inducing a current in the other. This sensor as well is easier to construct when large displacements are to be measured. Like the photosensor, it is a non-contact sensor, and it is relatively cheap, robust and easy to mount..

As discussed above, due to properties of the sensors and the flexure, the axes are intrinsically decoupled. Separate sensor elements are used to measure the x and y force components. Since the axes are decoupled, less electronics is needed, and calibration issues are much simpler.

2.2 Fewer degrees of freedom

In an instance where a human controls a robot with fewer than six degrees of freedom, the force sensor need not have six degrees of freedom. Fewer degrees of freedom means a simpler mechanical design, less electronics and wires, fewer sensor elements, and less calibration.

One benefit of the design, which follows partially from having fewer degrees of freedom, is the stiffness of the force sensor to large undesired force components.

For example, consider a person moving a heavy object suspended from an overhead rail system. Where does one put a force sensor to read the forces applied by the human? If one uses a handle, then the person must grab the device by the handle, even if it might be easier for the person to grasp the object directly. If one puts the force sensor between the object and the rail, then manipulating the object directly is allowed, but the force sensor must withstand the weight of the object. The force sensor presented here would be ideal for this problem, as it can withstand large forces out of the plane to be measured.

3. Design

3.1 Physical Overview

The force sensor is shown in figure 1. (The dimensions given in figure 1 are for the spring steel flexure.) The outer piece is the housing, while the handle is connected to the inner piece. Connecting the outer and inner pieces is a flexure element, best seen in the upper part of figure 2. The flexure itself is shown in the lower part of figure 2. As forces are applied to the handle, the flexure allows a displacement to occur between the two pieces. Due to the large aspect ratio of the flexure, it does not bend significantly in response to forces in the z-direction or torques about the x and y axes.

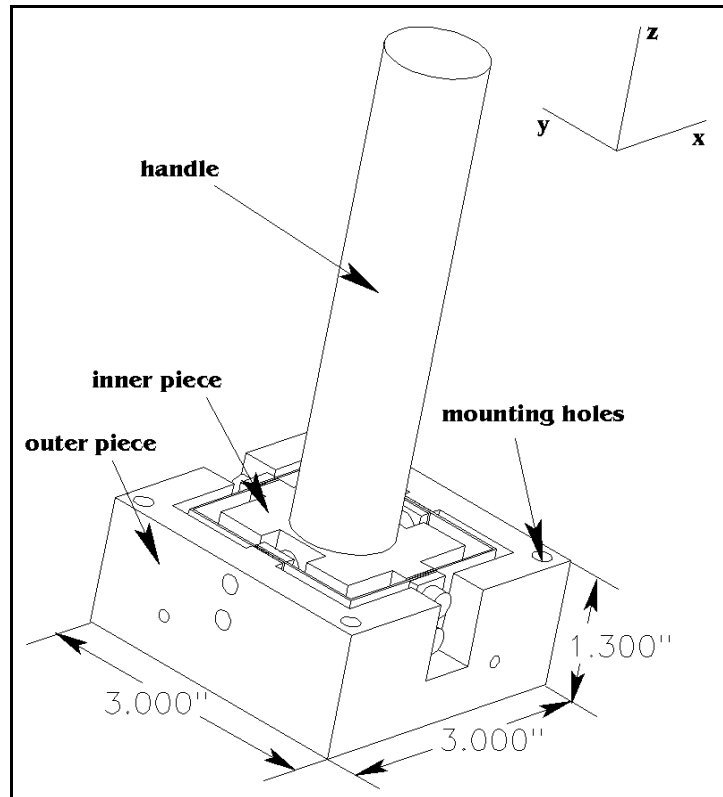


Figure 1

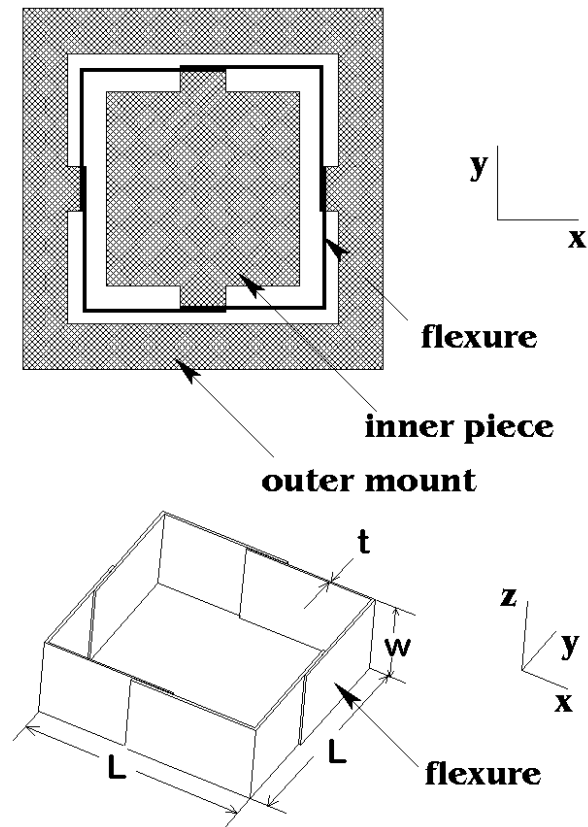


Figure 2

The flexure is designed to withstand approximately one millimeter of motion between the inner and outer pieces at which point the two pieces physically make contact preventing further motion. This protects the flexure from being broken.

Note the dimensions L , w , and t in figure 2. These dimensions are key to the design of the flexure and are used through much of the paper.

The displacement of the inner piece is measured using either optoelectronic or electromagnetic sensors.

3.1.1 Optoelectronic sensor

The optoelectronic sensors used are what are commonly referred to as infrared “reflective object” sensors. These sensors are mounted on a printed circuit board which is attached to the

inner piece. Light from an LED reflects off the inner wall of the outer piece and is detected by a photodiode, as shown in figure 3.

For each axis, there are two photosensors measuring the distance to the two walls of the outer object. The photosensors labeled A and B in figure 3, for example, are for measuring the x direction. These correspond to the photodiodes labeled A and B in figure 4.

Each LED actually shines on two photodiodes. Each photodiode produces a current proportional to the amount of light it receives. One photodiode, the reference, does not move with respect to LED, and is used to regulate the output of the LED. This significantly reduces the drift and temperature sensitivity of the circuit. This is the photodiode shown in the top part of figure 4.

The other photodiode receives light from the LED off the outer wall, as in figure 3. There are two of these photodiodes per axis. They are shown in the circuit in the bottom half of figure 4. These photodiodes measure the distance to the wall using the constant LED output. The difference in the amount of light received by these diodes causes a current, resulting in the voltage output. The output voltage is approximately linearly related to the displacement, for relatively small displacements. For the small deflections discussed here, the displacement is proportional to the force applied.

It was found for the photosensors used, Panasonic photo diode PN334 and infrared LED LN175, that a decent trade-off between sensitivity and linearity of the sensor response could be obtained if the maximum displacement allowed by the flexure was $\pm 1\text{mm}$.

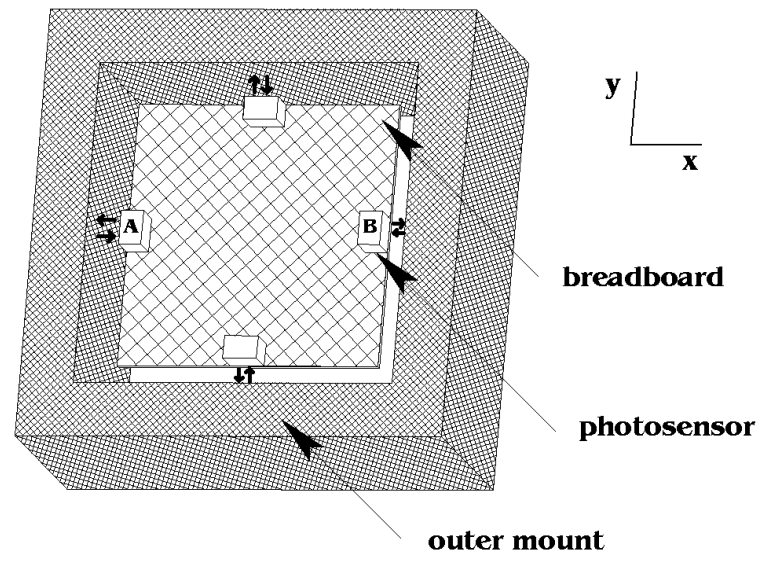


Figure 3

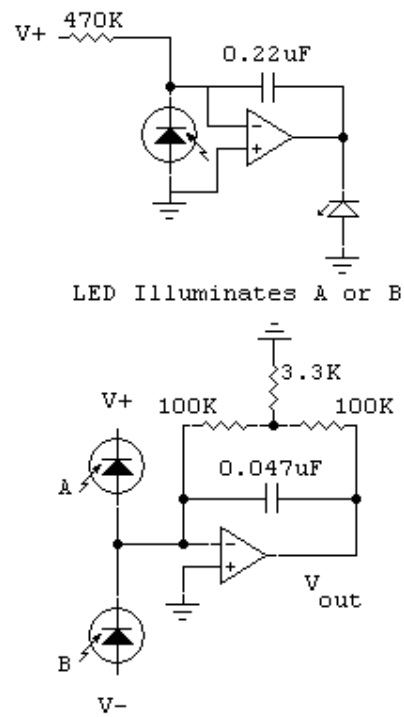


Figure 4

3.1.2 Electromagnetic sensor

The other displacement sensor used was the electromagnetic sensor. This sensor is shown in figure 5. We have two circuit boards mounted parallel to each other, one attached to the inner piece and one to the outer piece. When the flexure displaces in the x and y directions, due to the x and y components of the force, these two boards move relative to each other. The flexure can only displace significantly in the plane, so the boards will only slide by each-other, not getting significantly closer or farther.

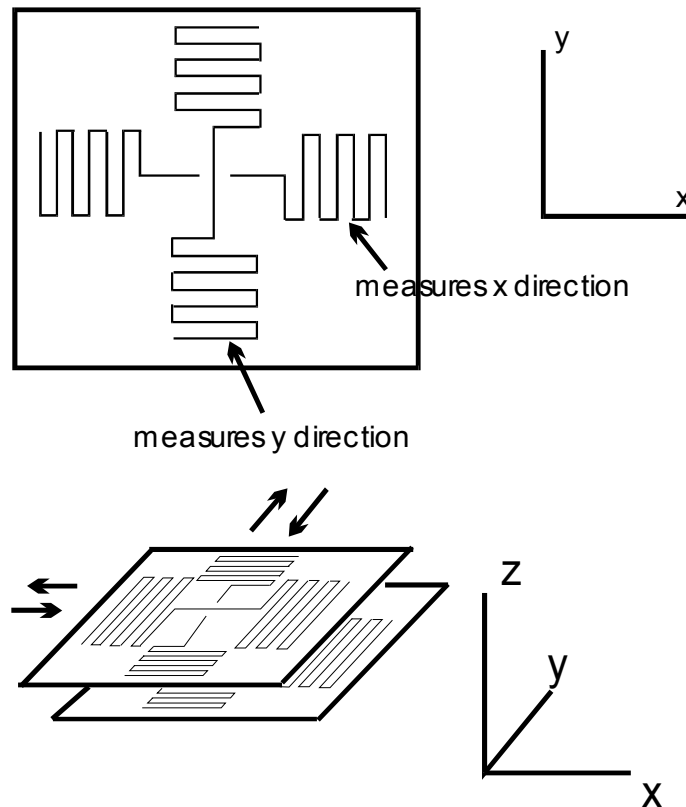


Figure 5

A zigzag conductive trace is put on each board. An alternating current is driven through the zigzag on one of the boards, which we will call the driving board. If the two zigzags of the two boards are perfectly lined up one on top of the other, the zigzag on the driving board will induce a current in the zigzag on the other board, which we will call the driven board. This is

because the changing current creates a changing magnetic field in the vicinity of each line of the zigzag on the driven board. This changing magnetic field creates an alternating voltage in the lines in the driven board. Note that all of these induced voltages will add up with one another.

If the two zigzags were shifted with respect to each other the width between two lines, then the current that the each conductive line on the driven board 'sees' on the driven board is the same magnitude and opposite sign. This is because the nearby conductive lines on the driving board have current going in the opposite direction as before. An AC voltage is induced, but its amplitude is the negative of the voltage induced before. Halfway in between these two locations, no voltage is induced. Thus the magnitude of the AC voltage can be used to determine the displacement of the two boards. Note that the relationship between displacement and voltage is not linear, but it will be linear for a small range.

One such zigzag is set up on each board for the x and y directions respectively, as shown in figure 5. Note that the sensor decouples the x and y axes. A displacement in the x direction causes no change in the voltage read in the y direction.

For the electromagnetic sensor, displacements considerably smaller than a millimeter may be measured. The displacement to be measured depends on the spacing of the zigzags on each board. A smaller displacement can result in smaller designs, as shown in the table in section 3.3.5.

3.2 Compliance matrix

The shape of the square flexure can be used to determine its compliance matrix. The flexure can be considered to be constructed of four identical L's (See figure 2). The compliance matrix of these L's is determined, assuming small deflections and simple stress distributions within the cross-section of the beam, as in [7]. The compliance matrix for one L is given below.

$$\begin{bmatrix}
 \frac{3}{4} & 0 & 0 & 0 \\
 \frac{1}{2} & 0 & 0 & 0 \\
 0 & a^2 \frac{3}{8} k & \frac{3}{4} a^2 \frac{3}{8} k & \frac{3}{4} a^2 \\
 0 & \frac{3}{4} a^2 \frac{3}{8} k & \frac{3}{2} a^2 \frac{3}{8} k & 0 \\
 0 & \frac{3}{4} a^2 & 0 & \frac{3}{2} a^2 \frac{3}{8} k \\
 \frac{3}{4} & 0 & 0 & 0
 \end{bmatrix}
 \quad (1)$$

$$\frac{L^3}{Et^3w} \underline{A} \underline{f} \quad \frac{L^3}{Et^3w} \underline{A} \underline{\vec{f}} \quad (2)$$

where $\Delta \vec{x}$ is the displacement, L is the length of one side of the square sheet, E , t , and w are the modulus of elasticity, thickness, and width of the material, $a^2=t^2/h^2$, $k = \frac{E}{G}$ is the ratio of the modulus of elasticity and the modulus of rigidity of the material, and \vec{f} is the applied force. Note that L has been chosen as the characteristic length for the angles and moments.

These compliance matrices are translated and rotated so that they are positioned as in figure 2 ([10]). Then the compliance matrix, C , is found by combining these four matrices by the following equation

$$\underline{C} = \underline{A}_i^{-1} \underline{k} \quad (3)$$

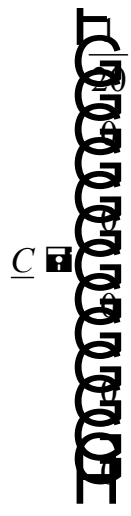
For the flexures described as above, we find that

$$\underline{C} = \begin{bmatrix} 0 & 0 & 0 & 0 & 0 \\ \frac{1}{20} & 0 & 0 & 0 & 0 \\ 0 & a^2 \frac{k(4a^2)}{4(k+4a^2)} & 0 & 0 & 0 \\ 0 & 0 & a^2 \frac{3(k+4a^2)(k+4a^2)}{12k^2+80ka^2+40a^4} & 0 & 0 \\ 0 & 0 & 0 & a^2 \frac{3(k+4a^2)(k+4a^2)}{12k^2+80ka^2+40a^4} & 0 \\ 0 & 0 & 0 & 0 & \frac{3}{112} \end{bmatrix} \quad (4)$$

$$\Delta \vec{x} = \frac{L^3}{Et^3 w} \underline{C} \vec{f}. \quad (5)$$

A number of insights can be gained from this compliance matrix. First, we notice that it is diagonal, which tells us that forces and torques create only their corresponding motions. This is due to the symmetry of the part. It also tells us how the choice of our aspect ratio parameter a^2 affects the design. If a^2 is small, then the flexure moves significantly only in response to the forces f_x , f_y , and τ_z . This is how the present design is made. However, if a^2 is large, then we have a flexure that responds to f_z , τ_x , and τ_y . Also we see how the dimensions of the flexure, L , t and w , matter.

We note that, for $t^2/w^2 \equiv a^2 \ll 1$, as in the present design, since k is of order 1, $a^2 \ll k$, and the compliance matrix simplifies further to



The diagram shows a vertical spring with a mass C attached to its top. A coordinate system is defined with the origin at the top of the spring, the x -axis pointing downwards, and the y -axis pointing to the right. The spring is represented by a vertical line with several loops. The mass C is a small square with a circle inside, positioned at the top of the spring.

$$\begin{matrix}
 0 & 0 & 0 & 0 & 0 \\
 \frac{1}{20} & 0 & 0 & 0 & 0 \\
 0 & \frac{a^2}{4} & 0 & 0 & 0 \\
 0 & 0 & \frac{a^2}{4} & 0 & 0 \\
 0 & 0 & 0 & \frac{a^2}{4} & 0 \\
 0 & 0 & 0 & 0 & \frac{3}{112}
 \end{matrix}
 \quad (6)$$

3.3 Decoupling of axes

Through a combination of the flexure (flexing element of force sensor) properties, the displacement sensor properties, and the design of the interface between the force sensor and the human, the measurement of the components of the forces becomes decoupled, allowing one displacement sensor per axis of force. The goal of this force sensor is to measure forces in a plane, or the f_x and f_y components of a force as shown in figure 6.

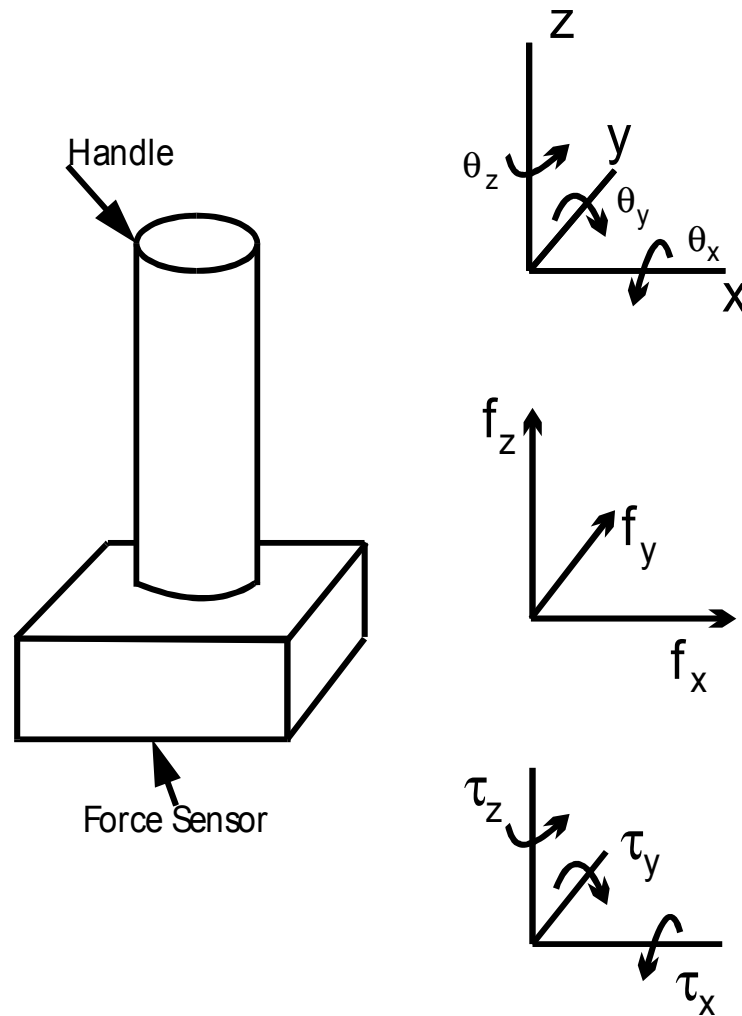


Figure 6

3.3.1 Flexure properties

In standard force sensors, the flexure is allowed to bend in all six available degrees of freedom. The specific force sensor presented here bends only in response to three of the six components of the applied force, the f_x , f_y and τ_z components, as shown in figure 6. The geometry of the flexure prevents significant bending in the other directions. This can be seen as a result of the compliance matrix of the flexure, which was discussed in the last section. Because the force sensor only deflects due to certain force components, the sensors designed to measure deflections will not be affected by the other force components.

3.3.2 Displacement sensor properties

The standard method for measuring the amount of bend in a flexure is to use strain gages. These are resistors whose resistance changes depending on the strain at the point of the flexure on which they are placed. However, with the larger displacement allowed in this design, new types of sensors become available. Two have been implemented so far. These are optoelectronic and electromagnetic sensors.

A major reason for choosing these kind of sensor is that deflections due to forces in the x direction do not affect the sensor elements designed to measure forces in the y direction. Thus the x and y forces are decoupled.

3.3.3 Human interface design

These sensors are less sensitive to τ_z forces than x and y forces, but this torque does cause an error. To minimize or eliminate this error, the interface between the human and the force sensor must be considered. The easiest method is to reduce the moment arm of the device. Another method is to have a ball bearing between the user and the device, to negate all such applied torques.

If these methods do not fit a design, another flexure should be used, such as the one in figure 10. This flexure only deflects in response to x and y forces and is not deflected by τ_z forces, and thus the axes are decoupled without considering the human interface. However, the design is not as simple to construct.

3.4 Parameter selection/Material selection

In this section, we will determine the size of the force sensor as well as the best materials to use. The general trend we find is that for any given applied forces, there is a minimum size

that the force sensor can be. So the question becomes, how small can I make my force sensor? As we will see, this depends on the material chosen.

In section 3.4.1, only in-plane forces (f_x , f_y , and τ_z) will be considered. This leads to some simple and insightful results. To simplify analysis, we assume that the parameter w has already been decided, and is assumed to be sufficient to prevent problems due to out of plane torques. This is the method that was used to decide parameters for the existing prototypes.

In sections 3.4.2 through 3.4.4, out of plane forces are considered as well (f_z , τ_x , and τ_y). We find that the sensor properties of the first section must be reevaluated. We determine equations for the amount of deflection caused by forces the flexure is designed to resist. We do a more thorough stress analysis, and determine new constraints on L and w required for the flexure not to break in response to a given applied force.

In section 3.4.5, these results are used to determine what values of L , t and w can be used in a design given certain applied forces. We find that regardless of the applied force there exist values of L , w , and t that satisfy all constraints. The parameters L and w determine the size of the flexure and thus the force sensor.

Finally, in section 3.4.6, we determine material properties that should be maximized when deciding the material with which to construct the flexure. We find that it is not clear that we have chosen the best materials, and some possible alternatives are listed.

3.4.1 In-plane force analysis

The flexure must be able to deflect a desired distance, x_d when the full scale force F is applied in the x (or y) direction. In addition, the flexure must not break at this deflection. The deflection as a function of force can be obtained from equation 5. It is

$$x_d \equiv \Delta x = \frac{1}{20} \frac{FL^3}{Et^3w} \quad (7)$$

where $F = f_x$ from equation 1. From simple mechanics of materials [7] type analysis, we find that the maximum moment M_{\max} , is related to the applied force by

$$M_{\max} = \frac{3}{40} FL \quad (8)$$

The moment of inertia, I , of the flexure when bent about the z-axis is

$$I = \frac{1}{12} wt^3 \quad (9)$$

We want the maximum stress to be a factor of safety less than the yield stress. The equation for the maximum stress is then

$$\sigma_{\max} = \frac{M_{\max}c}{I} = \frac{9}{20} \frac{FL}{wt^2} < \frac{\sigma_y}{F.S.} \quad (10)$$

where $c = t/2$ is the maximum distance from the normal axis of the flexure, σ_y is the yield stress, and F.S. is the factor of safety desired. From equations (7) and (10), we can find equations restricting the length L and thickness t of the material.

$$L < \frac{9}{\sqrt[3]{20}} \frac{(F.S.)x_d^{2/3} F^{1/3} E^{2/3}}{w^{1/3} \sigma_y} \quad (11)$$

$$t \geq \sqrt[3]{\frac{F}{20x_d E w}} L \quad (12)$$

We want to be able to make a sensor as small as is possible. This implies minimizing L . Thus we should choose a material that will minimize $E^{2/3}/\sigma_y$, or will maximize

$$\frac{\sigma_y^{3/2}}{E} \quad (13)$$

Certain materials score well by this criteria ([6]). One is high tensile strength steel such as the “spring steel” we have used. Other high scores are certain plastics, such as the Lexan used, and elastomers, such as rubber. Elastomers are probably not reasonable as the thickness, t , would have to be so large as to make the design unreasonable. Spring steel has good fatigue properties (when a F.S. of 2 or greater is used), but this may be a problem with plastics.

However, spring steel is difficult to machine and bend, as its hardness is similar to that of machine tools and it is rather brittle outside its elastic range.

We have made one force sensor prototype out of spring steel and the other out of Lexan. Spring steel has the difficulty of being difficult to machine and bend. Lexan is much easier to machine. However spring steel resists out of plane forces better. This is due to the modulus of elasticity of the material, as will be discussed in section 3.3.3.

For spring steel, F.S.=2, $x_d=1$ mm, $w=1.9$ cm, $F=294$ N, we find $L_{\min}=4$ cm. This is the value used in the spring steel prototype. Similarly, for Lexan, F.S.=2.4, $x_d=1$ mm, $w=2.5$ cm, $F=68$ N, $L=6.1$ cm.

3.4.2 More complete force analysis

We wish to be able to specify what parameters L , t , and w can be used given certain applied maximum forces that are to be read or resisted. The most general applied force consists of six components, f_x , f_y , f_z , τ_x , τ_y , and τ_z . See figure 6. However, since f_x and f_y have similar effects on the flexure, and τ_x and τ_y have similar effects on the flexure, and τ_z will be eliminated by the human interface, we need only analyze f_x , f_z , and τ_y . (The forces f_x and τ_y tend to exist together.) The force component f_x is the component to be measured. The other out of plane forces, f_z and τ_y , are to be resisted.

In the following sections, f_z and τ_y are considered to be the maximum force and torque applied in these directions. The force component f_x is considered to be the force in the x direction at which the flexure flexes the desired displacement x_d (set to 1mm for the prototypes built), at which point a physical stop is hit. Thus it is also the maximum force in the x direction that is exerted on the flexure.

In considering the impact of the forces to be resisted, there are two issues. One is how much will these forces bend the flexure. The other is whether these forces will break the flexure. For these two issues, we will find equations relating w and L to other parameters which can be considered constants, either being properties of the chosen material or design constraints.

3.4.3 Bending due to out of plane forces

As we shall see in the experimental section, bending due to out of plane forces causes errors in the force read-out. One can quickly determine how much a flexure bends due to a known applied force using equation 5 and plugging in the compliance matrix from equation 6. For the forces f_z and τ_y , these equations give

$$\theta_y = \frac{L}{4Et w^3} \tau_y, \quad \theta_z = \frac{L^3}{4Et w^3} f_z \quad (14)$$

Let's assume there exists a maximum allowable angular and positional displacement, $\Delta\theta_{x\max}$ and Δz_{\max} . Substituting equation (12) for t , and setting $\Delta\theta_x < \Delta\theta_{x\max}$, $\Delta z < \Delta z_{\max}$, we find

$$w \sqrt{\frac{5x_d \tau_y^3}{16E^2 f_x \theta_{y\max}^3}}, w L^{3/4} \sqrt{\frac{5x_d f_z^3}{16E^2 f_x z_{\max}^3}} \quad (15)$$

Thus we have restrictions on the parameter w . The only variable that relates to material properties in the above equation is E , the modulus of elasticity of the material. We see that to make the flexure small, we want a large value of E . This is a different requirement than equation 13. We see that in this respect spring steel is better than Lexan, and in general, metals are better than plastics. This is verified in the experimental section.

3.4.4 Stresses due to all applied forces

The components of the force we are considering (f_z , τ_x , and τ_y) cause stresses in the material. In determining what the maximum stress is in the material, we find that equation 10 becomes more complicated. With some elasticity analysis [7][9] and a few conservative approximations we find that

$$\sigma_{\max} \approx \frac{9}{20} \frac{L}{t^2 w} f_x \left(\frac{3}{4} \frac{L}{t w^2} \right) \left(f_z \frac{\tau_y}{L/2} \right) \frac{\sigma_y}{F.S.} \quad (16)$$

(See Appendix A, note that a similar method can be used for different flexure shapes.)

Note that this equation reduces to equation 10 when we neglect f_z and τ_y .

As before, we're combining an equation for the desired flexing of element, equation 7 still, with an equation for the stress on the element, now equation 16. As before, we use these to determine acceptable values for the parameters L , t , and w . (Before w was assumed to be known.) Note that L , t and w are the only unknowns in the equation. We plug equation 12, which is equivalent to equation 7, into equation 16. We then have an equation in the unknowns L and w . Solving this equation for L in terms of w and known constants, we get

$$L \geq \frac{\frac{3}{2} \frac{\tau_y}{c w^{2/3}}}{\left(\frac{9}{20} \frac{f_x}{c^2 w^{1/3}} + \frac{3}{4} \frac{\tau_y}{c w^{5/3}} + \frac{3}{8} \frac{f_z}{c w^{2/3}} \right) \sqrt{\left(\frac{9}{20} \frac{f_x}{c^2 w^{1/3}} + \frac{3}{4} \frac{\tau_y}{c w^{5/3}} + \frac{3}{8} \frac{f_z}{c w^{2/3}} \right)^2 + \frac{3}{4} \frac{\tau_y}{c w^{2/3}} \left(\frac{3 f_z}{2 c w^{5/3}} + \frac{\sigma_y}{F.S.} \right)}} \quad (17)$$

where

$$c = \sqrt[3]{\frac{2 f_x}{5 x_d E}}$$

This equation is not very nice, but it can be plotted, and some insight can be gained from it. One thing we can see is that as w becomes large, the minimum L becomes smaller. Thus there is a trade-off here. In the next section, we will take this relation between the parameters L and w and answer the question of what values for these parameters will create a flexure that will not break under predetermined applied loads.

3.4.5 Results, how to determine size parameters based on design constraints

We can take the inequalities that occur as a result of design parameters and plot them as functions between L and w . We can see what ranges of the parameters L and w can be used in the design. Then we can determine the parameter t from equation 12.

To obtain the plot, we need to know the following values: the material, and its modulus of elasticity E and yield stress σ_y ; the factor of safety $F.S.$, which is the ratio between the maximum stress in the flexure and the yield stress; the maximum displacement of the flexure, x_d , which is determined by the properties of your sensor and your desired force resolution (1mm has been typical for our designs); the force to be measured, f_x , and the other applied forces, f_z and τ_y , which are determined by the application.

Once we have these values, it's relatively straightforward to plug these values into the appropriate equations. The plots shown here were done in Mathematica, but other programs such as Matlab can be used. We plot equation 17 to determine for what values the flexure will break. If we wish, we can plot the two equations 15 to determine for what values the out of plane deflections will be small enough. And if necessary, we can plot the curve $t=\text{constant}$,

substituting in equation 12, if there is a minimum wall thickness that can be used, or if there are only discrete thicknesses available.

Let's do the above analysis for certain applied forces for both of the materials used so far, Lexan and spring steel. For spring steel, $E=200\text{GPa}$, $\sigma_y=1550\text{MPa}$. For Lexan, $E=2.5\text{GPa}$, $\sigma_y=60\text{MPa}$. Suppose the desired force range to be measured is 0-133N, this force is to be applied 5 cm from the flexure, causing a maximum torque of 6.8Nm, and a maximum vertical force (f_z) of 100 lbs. (440N) must be withstood without the device breaking.

For our factor of safety, we choose 2.4. Why? A factor of safety of 2 will, for both materials considered, allow stresses to reach the fatigue stress, which is the highest stress at which theoretically the material will not fatigue. We want a little more to incorporate other uncertainties. Other methods of choosing a factor of safety are possible.

We need to choose the maximum deflection of the sensor, x_d . For the optoelectronic sensor, we find that a reasonable compromise between linearity and resolution is found by letting $x_d=1\text{ mm}$.

Plugging all of these values into equation 17, we obtain the following plot.

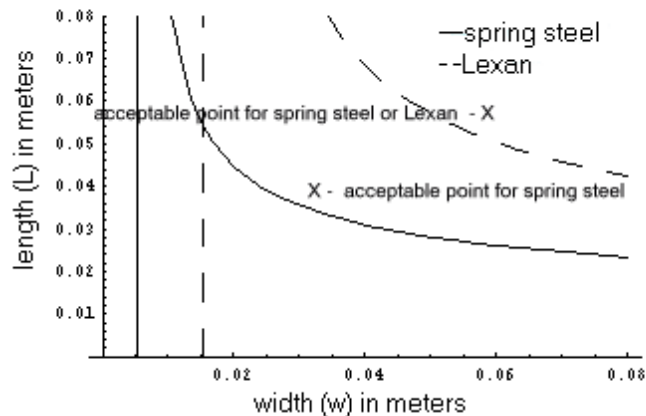


Figure 7

The vertical lines are asymptotes that show the minimum possible value that can be used for the width, w , regardless of the length, L .

Anything above a curve is an acceptable set of values for L and w . In general, a value along the curve will be chosen, as small values of L and w are desired in order to make the device small. We can plug in different values of w and find the corresponding values for L . For our example, reasonable values for spring steel are $L=4.6\text{cm}$, $w=1.9\text{cm}$. For Lexan $L=7.6\text{cm}$, $w=3.6\text{cm}$. Using equation 12, we find $t=.56\text{mm}$ for spring steel, and $t=3.19\text{mm}$ for Lexan.

With designs actually constructed as we have done, some simple assumptions (same placement of electronics, same electronics used, some machining issues for Lexan, reasonable thickness of outer piece, some strength issues at connection points for flexures to inner and outer pieces) leads us to an estimate of the size of the actual force sensor. (Different designs may improve these estimates.) We estimate the resulting steel force sensor to be 3"x3"x1 1/8", and the Lexan force sensor to be 5"x5"x1.75". We see that the steel force sensor is significantly smaller. However, the Lexan force sensor is much easier to construct.

Below is a table with various acceptable values for L and w for different applied forces. The factor of safety is 2.4 for all cases. Note that the maximum displacement affects the size of the force sensor. One can sacrifice resolution lost due to less deflection to obtain a smaller size.

material	f_x (N)	f_z (N)	τ_y (Nm)	x_d (mm)	w (cm)	L (cm)	projected size (cm x cm x cm)
Lexan	18	45	0.45	1	1.7	3.6	5.5x5.5x2.4
Lexan	18	45	0.45	0.5	1.4	2.8	4.7x4.7x2.1
spring steel	18	45	0.45	1	1.2	2.3	3.9x3.9x1.8
Lexan	133	440	6.8	1	3.6	7.6	12.7x12.7x4.4
Lexan	133	440	6.8	0.5	3.0	6.1	11.3x11.3x3.8
spring steel	133	440	6.8	1	1.9	4.6	7.6x7.6x2.8
spring steel	20	44500	13560	1	34	34	50x50x38(?)

The last example is extreme and demonstrates that for any input forces, a length and width can be found to measure these forces. Thus we can measure very small forces while resisting very large ones. We have to have a large flexure to do so, however. New flexure geometries may be useful in these cases.

3.4.6 Material considerations

The choice of material out of which to make the flexure is very significant in determining the overall dimensions of the device, as can be seen in the table in the last section. Certain materials clearly perform better than others. The properties of a material that are desired can be determined from the equations above, specifically equations 13, 15, and 16.

Equation 13 tells us that we should choose a material with a large value of

$$\frac{\sigma_y^{3/2}}{E} \quad (18)$$

A large value for this parameter allows a large amount of flex given a certain magnitude in-plane applied force.

However, this is not the only aspect of the flexure which is important. From equation 15, we see that for a material to not flex much in the out of plane direction, we wish to maximize the modulus of elasticity, E.

The third material property that should be maximized can be derived from equation 16. If, in this equation, we set $f_x=0$, and plug in equation 12 for the thickness t, we find that we can factor out a new material parameter that should be maximized. This parameter is

$$\frac{\sigma_y^3}{E} \quad (19)$$

A large value of this parameter gives a material that can withstand large out of plane forces without breaking.

Now that we have these 3 material properties ($\sigma_y^{3/2}/E$, σ_y^3/E and E) that we wish to maximize, we can use these to find out which materials are suitable for use. We can make a logarithmic plot of the yield stress σ_y versus the modulus of elasticity (Young's modulus) E . (The elastic limit is similar but is less than the yield stress σ_y , but since inelastic deformations are unacceptable in a force sensor, this is the material value that has been used and that needs to be considered.) It then turns out that lines of slope 3/2 give level curves for $\sigma_y^{3/2}/E$. Similarly lines of slope 3 give level curves for σ_y^3/E .

The plots below show all major types of existing materials and what ranges of values they have for these quantities. These plots are obtained from a program called CMS (Cambridge Material Selector) made by the company Granta Design Ltd. The first plot shows level curves for $\sigma_y^{3/2}/E$, the second for σ_y^3/E . Materials on the same level curve have the same value for the particular parameter being measured in the plot. Materials farther to the right have higher values for the parameters $\sigma_y^{3/2}/E$ and σ_y^3/E and materials higher on the plot have higher values of the modulus of elasticity, E .

In these plots, major material groups are given different colored ovals. Polymers are blue, natural materials are green, composites are light blue, metals are red, and ceramics are purple.

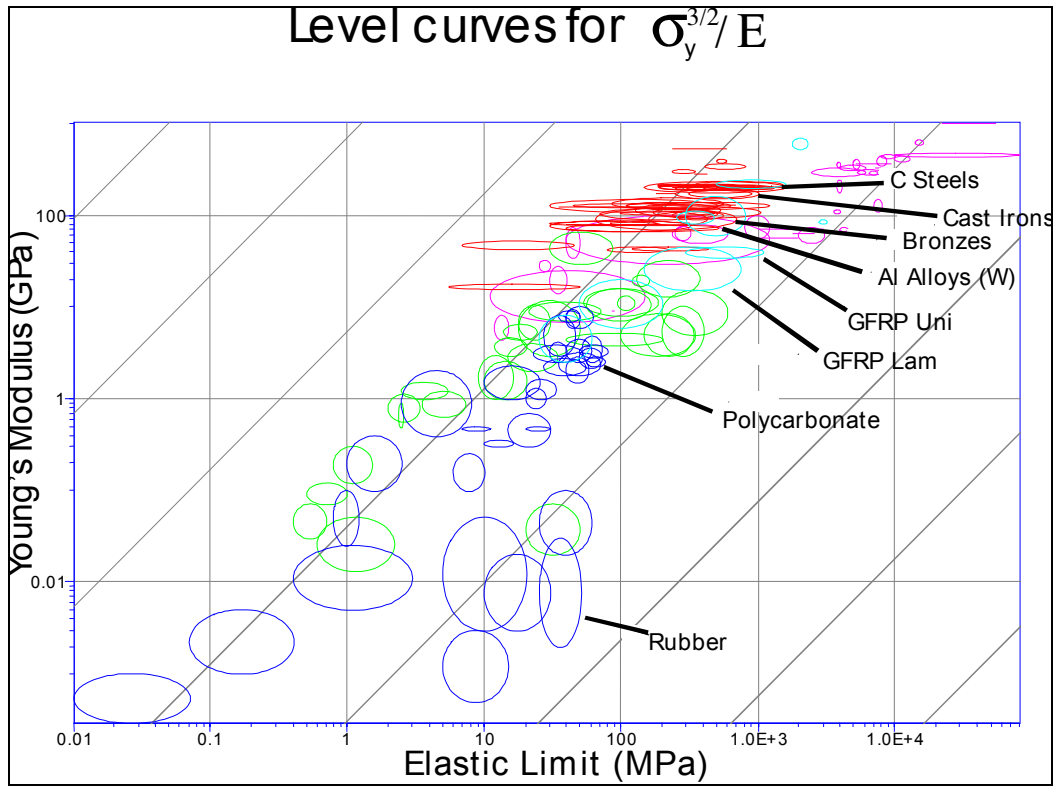


Figure 8

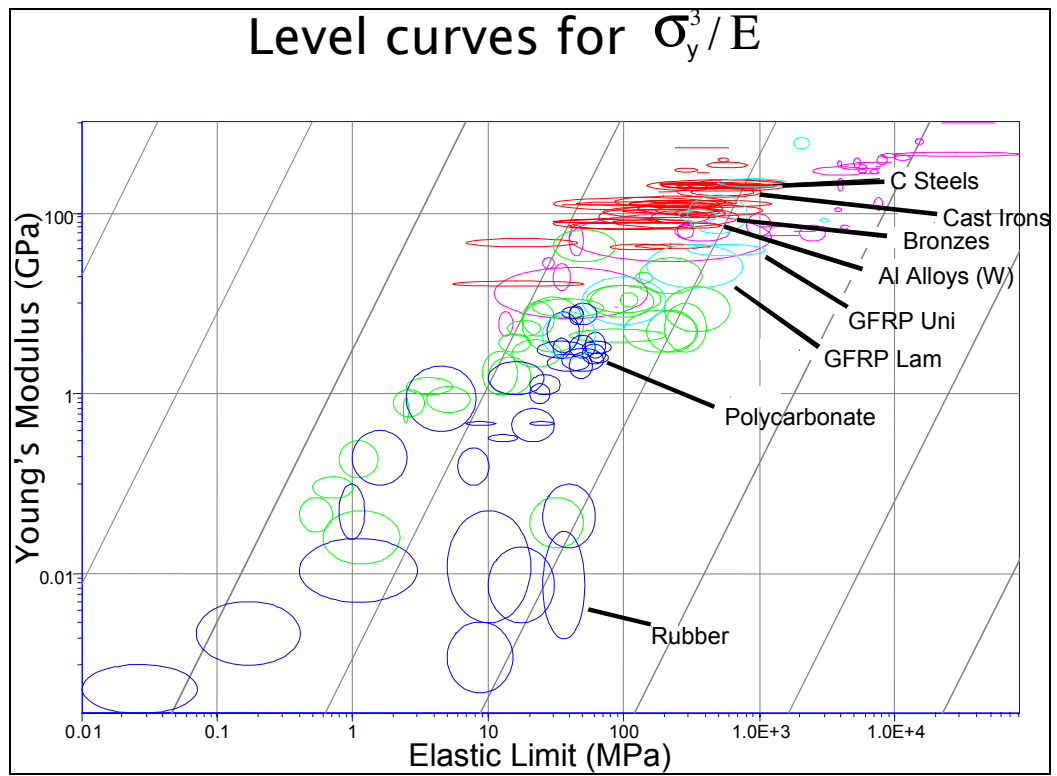


Figure 9

What can we deduce from these plots? The first thing to notice is that for the two materials that we have used, spring steel (high tensile strength carbon steel) and Lexan (polycarbonate), they have similar values for the parameter $\sigma_y^{3/2}/E$ but spring steel has a larger value for the parameter σ_y^3/E . Also, steel has a larger value of E . This tells us that while the materials will have similar in-plane flexing properties, spring steel will be able to better withstand and flex less in response to out of plane forces. This reduced out of plane flex is noted in the experimental section of this paper.

Clearly by these metrics spring steel is the better material. However, spring steel is hard to machine and bend, and can't be welded without losing its temper and thus its properties. When it is not welded but fastened, large forces can cause slip, causing an offset in the zero of the sensor. Lexan, on the other hand, is easy to machine, or even to injection mold. Thus while steel has better material properties, Lexan has much better fabrication properties.

In finding a material alternative to the ones used, it would be desirable to find a material that has the good material properties discussed above and also good fabrication properties. A few possibilities are listed in the figure, such as cast irons, bronzes, some wrought aluminum alloys, and fiberglass (GFRP). (Natural materials, such as silk, and ceramics have not been considered.) All of these materials have decent material properties. The ease of fabrication for these materials has not been explored.

As a final note, ceramics score very well by our material property considerations. This seems counterintuitive, and may not be reasonable due to fabrication issues. Also these materials are brittle, and a ductile material assumption was used in the analysis used to determine the above material parameters. Still, this is an interesting finding, and suggests that ceramics may be the best material for flexures of the type discussed here.

4. Alternative flexure designs

We can modify the present flexure by changing the position and shape of the legs of the flexure. This will change the properties of the flexure, but it will retain some basic properties. The distinguishing characteristic of the flexure chosen is that the elements of the flexure have a large aspect ratio. That is, they are much wider than they are thick. Any flexure designed like this allows motions in the plane (Δx , Δy , $\Delta \theta_z$) while preventing other motions (Δz , $\Delta \theta_x$, $\Delta \theta_y$).

In addition to this we can use different flexures that allow and prevent different motions. The idea behind the resulting force sensor is the same. Prevent some directions of motion, measure the other directions. (It seems reasonable to measure the other directions as orthogonally as possible.) To measure a torque, either a new or modified sensor should be introduced or linear motion a distance from the axis of twist would be measured.

A flexure which allows only x and y motion is shown in figure 10. It is two flexures in series, each of which allow only one degree of motion. This could be used if one needed to resist τ_z torque. In figure 10, the flexing elements labeled 1 allow flexing in the x direction, while the flexing elements labeled 2 allow flexing in the y direction.

Three flexures in series create the flexure in figure 11. This flexure allows motions in x, y and z, and prevents twists. The 'inner piece' would be attached to the four points labeled A. The 'outer piece' would be attached to the 2 points labeled B. The pairs of flexures labeled α , β , and γ allow the device to flex in the x, y and z directions respectively. Note that this design prevents buckling, which the design in figure 10 does not. However, the design has become complicated. A better idea for a flexure with these degrees of freedom is needed.

A flexure allowing only twist ($\Delta \theta_z$ in the figure) is shown in figure 12. The compliance matrix of this flexure has only one large element, relating $\Delta \theta_z$ to τ_z .

In all of these flexures, the sensors would have to be repositioned or modified to measure the different degrees of freedom. Note for example that the flexure in figure 11 could not use

electromagnetic sensing as we have presently done, as motion in the z direction would cause the 2 boards in figure 5 to approach each-other. The optoelectronic method would still work in this case. Motion in the y and z directions does not affect the reading in the x direction. Similar issues may arise with other flexures.

Many other flexures are, of course, possible. In choosing a flexure to use, we wish to find one that 1) only allows motions in the direction desired, 2) can be small and still allow large deflections in certain directions and prevent deflections in others, and 3) is as simple to make as possible.

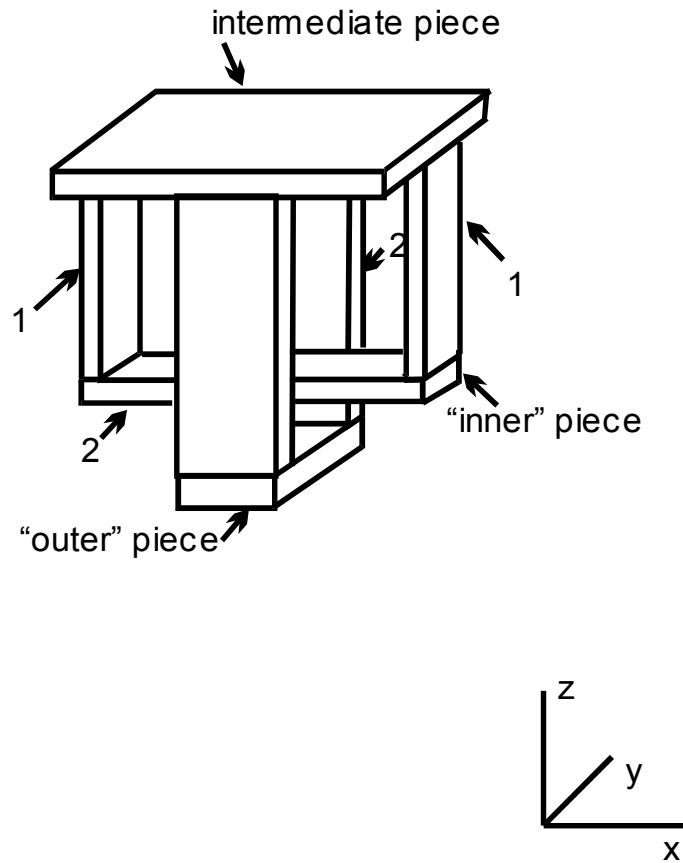


Figure 10

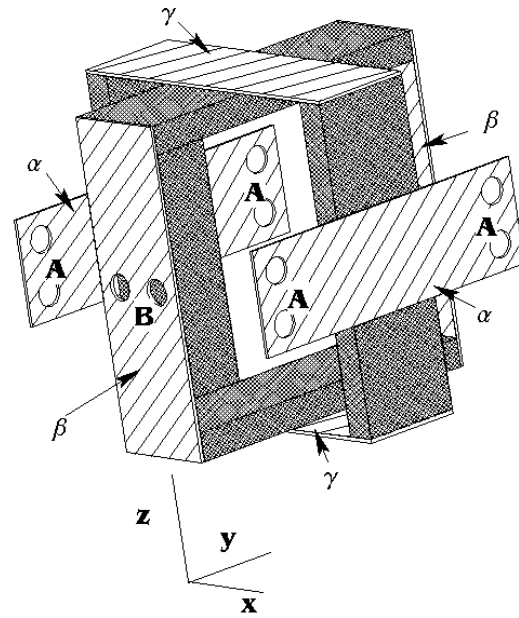


Figure 11
inner piece

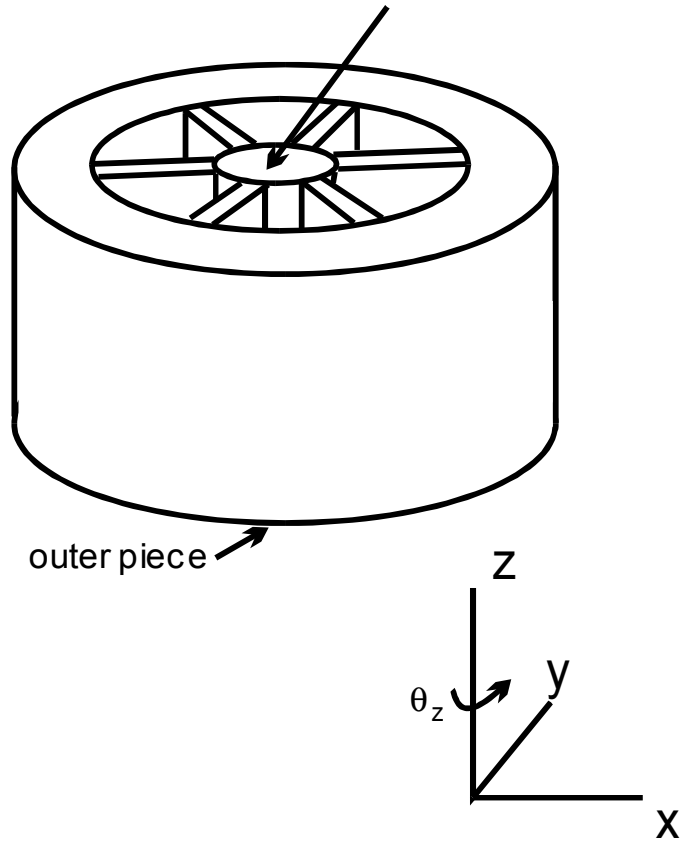


Figure 12

5. Experimental Results

The force sensors described above have been built and calibrated. It has been compared to an existing force sensor, the ATI Gamma model 6 axis force sensor. Results comparing these two sensors are summarized in the table below.

	<i>ATI</i>	<i>Two-axis optical spring steel</i>	<i>Two-axis optical Lexan</i>	<i>Two-axis electromagnetic Lexan</i>
Max force(f_x) (Newtons)	65	170	68	22.4
Max displacement (millimeters)	0.0074	0.60	1.0	0.33
Sensitivity, Volts/N	0.0734	0.010	0.0425	0.0533
Long term drift, % of full scale in 24 hours	0.10%	(1.5%)*	0.90%	1.07%
Short term drift, % of full scale in 5 minutes	0.025%	(0.047%)*	0.028%	0.034%
Maximum nonlinearity	not measured	(0.5%)*	1.25%	2%
Ratio of response to $\tau_y/2.5\text{cm}$ to response to f_x	NA	0.01	0.065	not measured

*-calculated, not measured

5.1 Deflection

The maximum deflection of the two-axis spring steel sensor was 0.60 mm (in either direction). This required a force of 170 N. This is very close to the force expected from the theory, which is 177 N. For the Lexan force sensor the maximum deflection occurred around 68 N. This is close to the 60 N predicted in theory.

5.2 Noise and drift

All drift terms above are in terms of peak to peak measurement. Short-term noise was significantly less than the drift terms given in the above. This is after both digital and analog filtering using a time constant of approximately 0.1 seconds. This time constant is reasonable for human interaction, but may be too large for other applications. In this case, the noise contribution would have to be reevaluated.

The five minute drift is the amount the measured force varies in five minutes for a constant applied force, and is much less than the long term drift. For applications involving humans interacting with the sensor, forces tend to be applied for short periods of time.

Note that for both the optoelectronic and the electromagnetic sensors, the five minute drift is similar to that of the ATI force sensor. However, the long term drift is approximately ten times larger for both. This still gives adequate resolution for many applications.

However, the long-term drift in these tests was monotonic and exponentially decaying. This suggests settling of some kind, possibly of the Lexan flexure itself. This must be tested. The drift does not seem random and may be eliminated, promising even greater resolution.

5.3 Linearity

Linearity results for the two sensors were very promising. The output for the two sensors is shown in the graphs below. One can see for the optoelectronic sensor, the voltages start to trail off at high forces. This is when the physical stop is met, hindering further motion.

For the electromagnetic circuit, the output steadily becomes increasingly nonlinear. One can then choose a range as a compromise between linearity and resolution. In this case, a maximum nonlinearity of 2% was chosen. If so desired, nonlinearities can be compensated for by extra calibration, but for the small values found here, this should not be necessary.

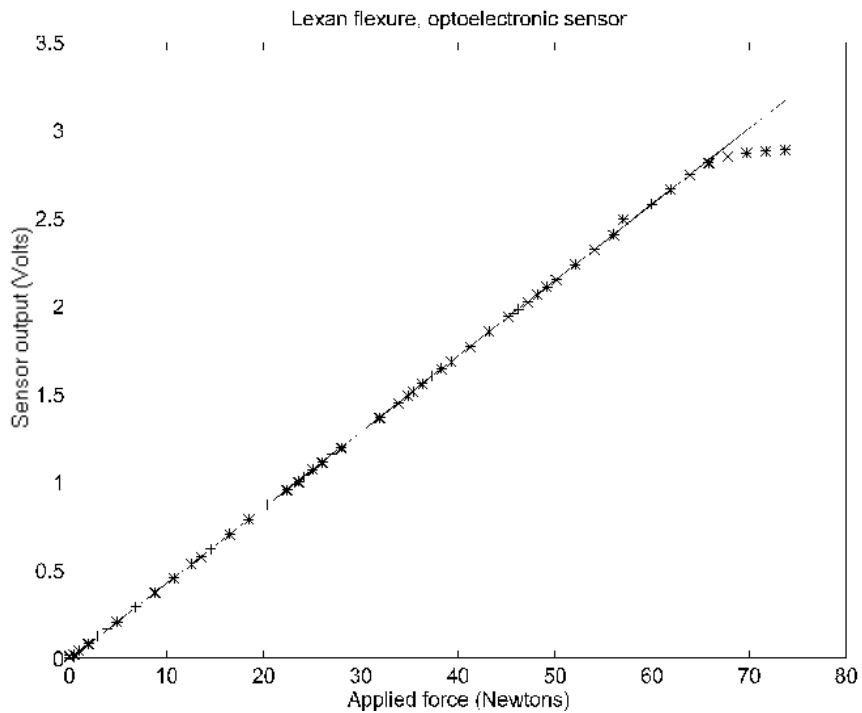


Figure 13

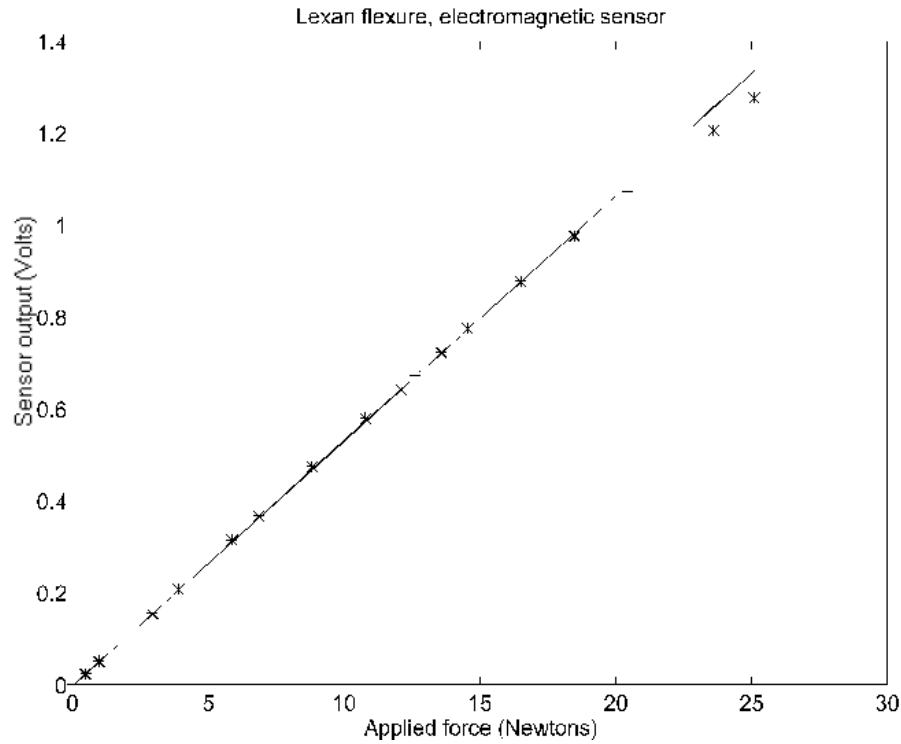


Figure 14

5.4 Response to out of plane forces

For the spring steel force sensor, forces (and torques) applied to the device in the z , τ_x , and τ_y directions caused very small but measurable changes in the measured force. For the Lexan sensor, there was more sensitivity to these forces.

For the Lexan force sensor, a difference of 6.5% is measured in an applied force f_x if it is applied to two locations an inch apart. This is a large error, and may in some cases be unacceptable. The flexure would then have to be designed to flex less in the $\Delta\theta_y$ direction, as discussed in section 3.3.3.

For the spring steel force sensor, a difference of approximately 1% is measured under the same conditions. This seems better. But again, if this is unacceptable, the flexure can be designed to perform any amount better by reducing the flex $\Delta\theta_y$ as discussed in section 3.3.3. As with all design improvements mentioned, it will increase the size of the force sensor.

A torque in the τ_z direction does cause a measured force in the x-y plane. For the spring steel sensor, a torque of 0.5 Nm caused a recorded force change of 9.8 N. This seems tolerable for a hand-held device, where the characteristic length is on the order of 2 to 3 cm, but could be troublesome in other applications.

5.5 Experimental summary

The ATI force sensor outperforms the two-axis sensor in long term resolution, however in many applications its high performance may not be needed. The present long-term drift looks suspiciously like some kind of settling and its source will have to be determined.

The spring steel force sensor has better resistance to out of plane forces. This is due to the mechanical properties of spring steel, and the geometries of the flexures chosen.

There was little nonlinearity in either the optoelectronic or electromagnetic circuit. For the electromagnetic circuit, the maximum displacement can be chosen to limit nonlinearity, at the cost of resolution.

We intend to further increase the sensitivity and reduce the noise and drift levels of the two-axis sensor.

6. Summary

A new force sensor design was described in this paper. It is much cheaper and easier to construct than existing commercial force sensors.

This force sensor differs in many respects from conventional force sensors. The relaxed design requirements of human-robot interaction allows for new design innovations. The reduced degrees of freedom allows a different class of flexures to be used. The greater allowable compliance in human/robot applications makes the force sensor easier to construct. In addition it allows the use of new types of sensors elements. Two such sensor elements, optoelectronic and electromagnetic, have been used.

The force sensor consists of a flexure and a displacement sensor. The flexure allows motions in certain directions due to certain components of the applied force and prevents motions in other directions. The displacement sensor measures the distance displaced, and thus the force, in the allowed directions. The combination of this class of flexures and photosensors allows the axes to be orthogonal, simplifying sensor placement, electrical design, and calibration.

BIBLIOGRAPHY

- [1] J. E. Colgate, W. Wannasuphoprasit, and M. A. Peshkin, "Cobots: Robots for Collaboration with Human Operators," Proc. 1996 ASME Int. ME Cong. and Exhib., Atlanta, GA, DSC-Vol. 58, pp. 433-39.
- [2] W. Wannasuphoprasit, R. B. Gillespie, J. E. Colgate, M. A. Peshkin, "Cobot Control," Proc. 1997 IEEE Int. Conf. on R&A, Albuquerque, NM, pp. 3571-3577.
- [3] O. M. Al-Jarrah and Y. F. Zheng, "Arm-Manipulator Coordination for Load Sharing Using Compliant Control," Proc 1996 Int. Conf on R&A, Columbus, OH, pp. 1000-1005.
- [4] K. I. Kim and Y. F. Zheng, "Human-robot Coordination with Rotational Motion," Proc. 1998 IEEE Int. Conf. on R&A, Leuven, Belgium, pp. 3480-3485.
- [5] A.K. Bejczy and Z.F. Szakaly, "A harmonic motion generator(HMG) for telerobotic applications," Proc. 1991 IEEE Int. Conf. on R&A, Sacramento, CA, 1991, pp. 2032-2039.
- [6] M.F. Ashby, "Material Property Charts" ASM Handbook Vol. 20, pg. 266-280, ASM International, 1997.
- [7] F. P. Beer and E. R. Johnston, Jr., Mechanics of Materials, McGraw-Hill, 1976
- [8] John A. Hilton, "Force and Torque Converter" United States Patent 4,811,608, 1989
- [9] S. P. Timoshenko and J. N. Goodier, Theory of Elasticity, McGraw-Hill, 1951
- [10] Richard P. Paul, Robot Manipulators: Mathematics, Programming, and Control, MIT Press, 1981

Appendix

In the appendix, we will show how to derive equation 17. The steps are as follows.

- 1) Find the stresses in a cross-section of an element as a function of the force applied to the element.
- 2) Estimate the maximum stress in an element of the flexure as a function of the force applied to the element.
- 3) Determine the applied force on an element from the applied force on the entire flexure.
- 4) Use these to estimate the maximum stress in the flexure as a function of applied force.

Step 1)

The flexure is made of 4 L-shaped elements, such as that shown in figure 2. We will analyze one such element. Suppose a force is applied to one end of the element, as shown in figure 15. Some terminology must be introduced here. A force (or torque) with an L superscript, such as f_x^L or τ_z^L , is a force applied at the end of the flexure. A force with a s superscript, such as f_x^s , is the force applied on a cross-section a distance s along the flexure, where s is a variable. A force without such a superscript, such as τ_y , is a force applied to the entire flexure.

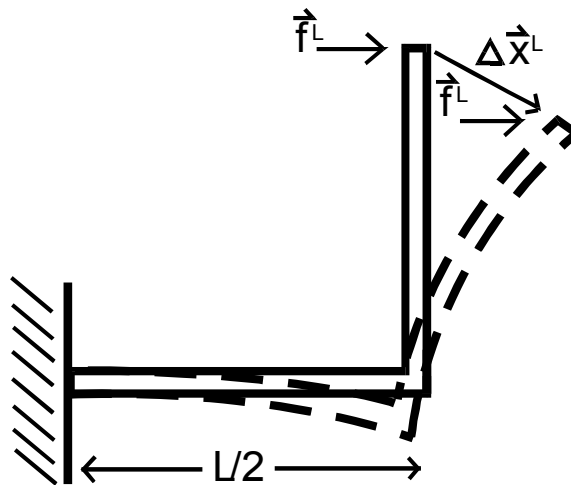


Figure 15

Using a free body diagram, the torque applied to any cross-section can be determined, as shown in figure 16. From this, using the equations of equilibrium, we get the equations for the force and torque applied to any cross-section of the flexure.

$$\begin{aligned}
 f_x^s &= f_x^L \\
 f_y^s &= f_y^L \\
 f_z^s &= f_z^L \\
 \tau_x^s &= \tau_x^L - f_z^L (L/2), s \leq L/2 \\
 \tau_x^s &= \tau_x^L - f_z^L (L - s), s > L/2 \\
 \tau_y^s &= \tau_y^L - f_z^L (L/2 - s), s \leq L/2 \\
 \tau_y^s &= \tau_y^L, s > L/2 \\
 \tau_z^s &= \tau_z^L - f_x^L L/2 - f_y^L (L/2 - s), s \leq L/2 \\
 \tau_z^s &= \tau_z^L - f_x^L (s - L/2), s > L/2
 \end{aligned} \tag{A1}$$

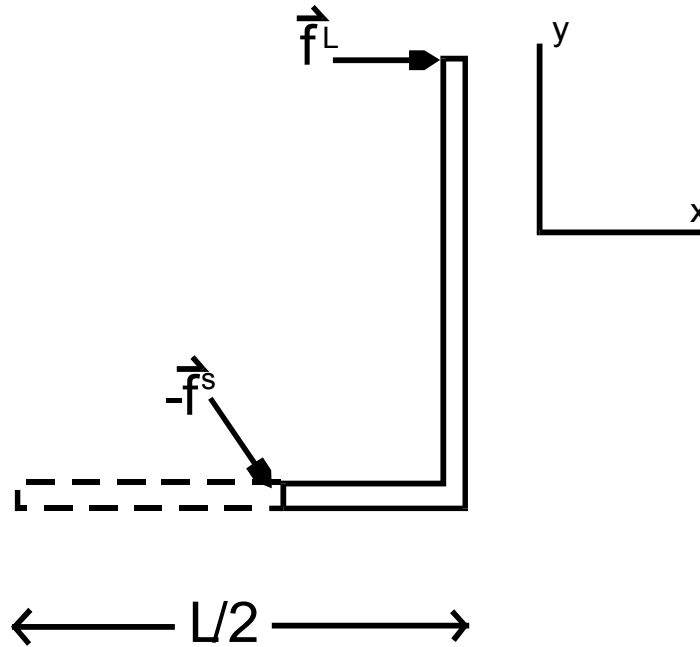


Figure 16

Step 2)

We determine the stress distribution using local coordinates. The global coordinates are the x , y and z directions mentioned above. We call the local coordinates x' , y' and z (this is because the z direction agrees between local and global coordinates). See figure 17.

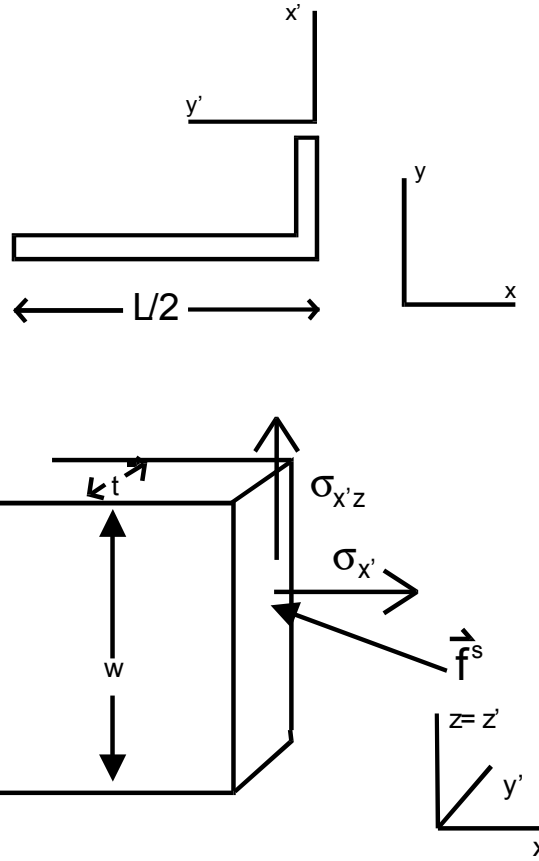


Figure 17

For each force applied to a cross-section, there is a corresponding stress distribution. Here a couple of conservative simplifying assumptions are made. Each stress distribution has a maximum somewhere in the cross-section. We assume all of these maximums occur at the same location in the cross-section. Next, we neglect shearing stresses in the $\hat{\sigma}_{x'y'}$ direction, assuming all shearing stresses are in the same direction. Now our maximum stress $\vec{\sigma}$ can be found in terms of the stress unit vectors $\hat{\sigma}_x$, the normal stress, and $\hat{\sigma}_{x'z}$, the shear stress. The maximum stress, $\vec{\sigma}^s$, is a function of s, the location of the cross-section, but because of our assumptions, is not a function of where we are in the cross-section.

The maximum stress, $\vec{\sigma}^s$, is a sum of the stresses caused by each of the applied forces and torques. We can write this as

$$\vec{\sigma}^s = \vec{\sigma}_{f_x^s} + \vec{\sigma}_{f_y^s} + \vec{\sigma}_{f_z^s} + \vec{\sigma}_{\tau_{x'}^s} + \vec{\sigma}_{\tau_{y'}^s} + \vec{\sigma}_{\tau_z^s} \tag{A2}$$

We neglect tensile and shear stresses caused by the force components f_x and f_y . In general, forces cause less stresses (are of higher order) than moments. The force component f_z is still considered, because there are instances when the force component f_z is very large compared to other applied forces and torques. Standard elasticity analysis gives us a value for the maximum stress due to each of these applied forces. We find ([7],[9])

$$\begin{aligned}
 \vec{\sigma}_{f_z^s} &= \frac{3 f_z^s}{2 w t} \hat{\sigma}_{x'z} \\
 \vec{\sigma}_{\tau_{x'}^s} &= \frac{3 \tau_{x'}^s}{w t^2} \hat{\sigma}_{x'z} \\
 \vec{\sigma}_{\tau_{y'}^s} &= \frac{6 \tau_{y'}^s}{w^2 t} \hat{\sigma}_{x'} \\
 \vec{\sigma}_{\tau_{z'}^s} &= \frac{6 \tau_{z'}^s}{w t^2} \hat{\sigma}_{x'}
 \end{aligned} \tag{A3}$$

This leads to

$$\vec{\sigma}^s = \left(\frac{6 |\tau_z^s|}{w t^2} + \frac{6 |\tau_{y'}^s|}{w^2 t} \right) \hat{\sigma}_x + \left(\frac{3 |f_z^s|}{2 w t} + \frac{3 |\tau_{x'}^s|}{w t^2} \right) \hat{\sigma}_{xz} \tag{A4}$$

The absolute value signs ensure that these terms do not subtract from each-other. In reality, there are certain areas on the cross-section where the sections add and others where they cancel. Since we want the maximum stress, we use absolute values.

Now we make two substitutions. First, we change to global coordinates. For our flexures this is relatively simple. For $s < L/2$, $x' = x$, $y' = y$. For $s > L/2$, $x' = y$, $y' = -x$. Second, we substitute in equation A1 for the forces. We obtain

$$\begin{aligned}
\vec{\sigma}^s &= \left(\frac{6}{wt^2} \left| \tau_z^L \oplus f_x^L L / 2 \oplus f_y^L (L / 2 \oplus f_z^L) \right| \oplus \frac{6}{wt^2} \left| \tau_y^L \oplus f_z^L (L / 2 \oplus f_x^L) \right| \oplus \frac{3}{2wt} \left| f_z^L \right| \oplus \frac{3}{wt^2} \left| \tau_x^L \oplus f_z^L L / 2 \right| \right) \vec{\sigma}_{x,z} \\
& \quad s \oplus L / 2 \\
\vec{\sigma}^s &= \left(\frac{6}{wt^2} \left| \tau_z^L \oplus f_x^L (s \oplus f_z^L) \right| \oplus \frac{6}{wt^2} \left| \tau_x^L \oplus f_z^L (L \oplus f_x^L) \right| \oplus \frac{3}{2wt} \left| f_z^L \right| \oplus \frac{3}{wt^2} \left| \tau_y^L \right| \right) \vec{\sigma}_{x,z} \\
& \quad s \oplus L / 2
\end{aligned} \tag{A5}$$

Step 3)

We see that the deflection of the flexure is related to the force by equation 5.

$$\Delta \vec{x} = \frac{L^3}{Et^3 w} \underline{C} \vec{f} \tag{5}$$

The matrix \underline{C} is the compliance matrix for the entire flexure. Let the matrix \underline{A} be the compliance matrix for one of the legs of flexure. A similar relation exists for the matrix \underline{A} .

$$\vec{x}^L = \frac{L^3}{Et^3 w} \underline{A} \vec{f}^L \tag{A6}$$

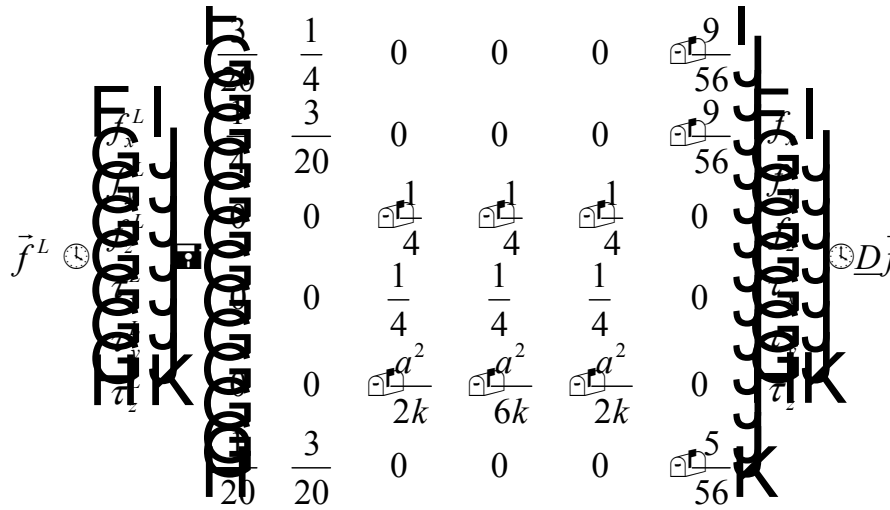
Note a couple of things about this equation. The displacement is due to the force on the leg of the flexure, denoted as \vec{f}^L . The displacement of each leg of the flexure is the same as the displacement of the entire flexure. Thus

$$\vec{x}^L = \vec{x} \tag{A7}$$

Combining these equations gives

$$\vec{f}^L = \underline{A}^{-1} \underline{C} \vec{f} \tag{A8}$$

There are also translations and rotations of the legs of the flexure involved in the derivation of equation 5 and equation A8 ([10]). These are relatively simple. For our geometry, we find that



$$\begin{array}{cccc}
 \frac{1}{4} & 0 & 0 & 0 \\
 \frac{3}{20} & 0 & 0 & 0 \\
 0 & \frac{1}{4} & \frac{1}{4} & \frac{1}{4} \\
 0 & \frac{1}{4} & \frac{1}{4} & \frac{1}{4} \\
 0 & \frac{a^2}{2k} & \frac{a^2}{6k} & \frac{a^2}{2k} \\
 \frac{3}{20} & 0 & 0 & 0
 \end{array}
 \quad (A9)$$

where we call this substitution matrix \underline{D} , and $a^2=t^2/h^2$, $k = \frac{E}{G}$, as before. We have used the fact that $a^2 \ll 1$ to simplify the above matrix.

Step 4)

We want the maximum stress in the flexure. First we find the stress, $\bar{\sigma}^s$, in terms of forces on the flexure by substituting equation A9 into equation A5. Since the forces f_x and f_y act similarly on the flexure, and similarly so do the torques τ_x and τ_y , and since we are assuming τ_z is small or is accounted for mechanically, we can set $f_y=\tau_x=\tau_z=0$. We find an expression for $\bar{\sigma}^s$ which is clearly maximum at $s=0$. These simplifications lead to the following expression for the stress (again using fact that $a^2 \ll 1$)

$$\bar{\sigma}_{\max} = \left(\frac{9L}{20wt^2} |f_x| + \frac{3L}{4w^2t} \left| f_z - \frac{\tau_x}{L/2} \right| \right) \hat{\sigma}_{x'} + \left(\frac{3}{8tw} \left| f_z - \frac{\tau_x}{L/2} \right| \right) \hat{\sigma}_{xz} \quad (A10)$$

where we have removed the s superscript (since we found the maximum value at $s=0$) and added a max subscript to denote that this is the maximum stress in the flexure.

The material is assumed to be ductile. This means it will fail in shear. The formula for the maximum shear is

$$T_{\max} = \sqrt{\frac{G}{2} k \sigma_{xz}^2} \leq \frac{T_y}{F.S.} \leq \frac{\sigma_y}{2F.S.} \quad (\text{A11})$$

Here the fact is used that for the materials considered, (and for most ductile materials) the shear yield strength is approximately half the tensile yield strength. For other materials this can be altered. We can approximate equation (A11) with the inequality

$$\sqrt{\frac{G}{2} k \sigma_{xz}^2} \leq \frac{\sigma_x}{2} \leq \sigma_{xz} \quad (\text{A12})$$

This is used to simplify the final results. This approximation is most conservative when the two terms are of similar magnitudes. The analysis can be done without this approximation, it just becomes less manageable. Combining equations (A10)-(A12) we get

$$\frac{9}{20} \frac{L}{t^2 w} f_x \leq \frac{3}{4} \left(\frac{L}{tw^2} \leq \frac{1}{tw} \right) (f_z \leq \frac{\tau_x}{L/2}) \leq \frac{\sigma_y}{F.S.} \quad (\text{A13})$$

This is equation 16 so we are done.

Note that the above analysis can be modified at many points as far as what approximations are made. A more exact answer can be obtained at the cost of computational complexity. Note also that the above analysis transfers straightforwardly to other flexure shapes.